

Article

# Comparison of Cooling Methods for a Thermoelectric Generator with Forced Convection

Young Hoo Cho <sup>1</sup>, Jaehyun Park <sup>2</sup>, Naehyuck Chang <sup>1</sup> and Jaemin Kim <sup>3,\*</sup>

<sup>1</sup> School of Electrical Engineering, Korea Advanced Institute of Science and Technology, 291, Daehak-ro, Daejeon 34141, Korea; [younghoo@cad4x.kaist.ac.kr](mailto:younghoo@cad4x.kaist.ac.kr) (Y.H.C.); [naehyuck@cad4x.kaist.ac.kr](mailto:naehyuck@cad4x.kaist.ac.kr) (N.C.)

<sup>2</sup> School of Electrical Engineering, University of Ulsan, Ulsan 44610, Korea; [jaehyun@ulsan.ac.kr](mailto:jaehyun@ulsan.ac.kr)

<sup>3</sup> Department of Electronics Engineering, Myongji University, Yongin 17058, Korea

\* Correspondence: [jaemin@esl.mju.ac.kr](mailto:jaemin@esl.mju.ac.kr); Tel.: +82-31-330-6373

Received: 22 May 2020; Accepted: 13 June 2020; Published: 19 June 2020



**Abstract:** A thermoelectric generator (TEG) is a clean electricity generator from a heat source, usually waste heat. However, it is not as widely utilized as other electricity generators due to low conversion efficiency from heat to electricity. One approach is a system-level net power optimization for a TEG system composed of TEGs, heat sink, and fans. In this paper, we propose airflow reuse after cooling preceding TEGs to maximize system net power. For the accurate system net power, we model the TEG system, air, and heat source with proper dimension and material characteristics, and simulate with a computational fluid dynamics program. Next, the TEG power generation and the fan power consumption are calculated in consideration of the Seebeck coefficient and internal electrical resistance varying with hot and cold side temperatures. Finally, we find the optimal number of TEGs and fan speed generating the most efficient system net power in various TEG systems. The results show that the system with a side fan with a specific number of TEGs provides a system net power up to 58.6% higher than when with a top fan. The most efficient system net power with the side fan increases up to four TEGs generating 1.907 W at 13,000 RPM.

**Keywords:** system-level optimization; net power; thermoelectric generator; forced convection; computational fluid dynamics (CFD)

## 1. Introduction

A thermoelectric generator (TEG) is a device composed of pairs of P-type (hole-conducting) and N-type (electron-conducting) thermoelectric elements [1] and there are three kinds of TEG technologies: lateral/lateral, vertical/lateral, vertical/vertical [2,3]. We target for vertical/vertical and vertical/lateral TEG devices that heat flows from side to side in vertical. Both sides typically consist of two thin ceramic plates in vertical/vertical and vertical/lateral TEGs. TEG is a promising energy harvester because it only requires a temperature difference across the thermoelectric elements to produce electricity. According to the Seebeck effect, the TEG produces more electricity with the more temperature difference on the two ceramic plates. Moreover, it has a relatively low maintenance cost compared with such generators with rotating parts creating noise or vibration. However, the TEG is not as popular as other generators due to its conversion efficiency. A TEG efficiency is up to about 10% with the development of new thermoelectric materials and efficient modules [4]. In contrast, the conversion efficiency of other renewable energy generators, such as a photovoltaic cell and a wind generator, is more than 15%. So, many studies tried to increase TEG performance in material or system-level.

The thermoelectric material is a key component of TEG efficiency, and Tin Selenide (SnSe) shows an outstanding performance compared with other materials [5]. Graphdiyne has a high electrical conductivity, the large Seebeck coefficient, and low thermal conductivity, so TEG based on graphdiyne

shows a high figure of merit at room temperature [6]. In bismuth telluride-based alloys used popularly, high figures of merit for p-type ( $\text{Bi}_{0.5}\text{Sb}_{1.5}\text{Te}_3$ ) and n-type ( $\text{Bi}_2\text{Te}_{2.7}\text{Se}_{0.3}$ ) are reported with ZT 1.86 at 320 K and ZT 1.20 at 445 K [7,8]. Even though TEG with improved materials provides a high performance, it is seldom used with single TEG due to its limited power generation capacity and its size.

Many applications, such as automobiles [9–11], a chimney [12], and a human body [13], apply multiple TEGs in parallel and/or series connection for the higher TEG-harvested power because they have a large surface area, where one TEG cannot efficiently convert all the heat energy to electricity. However, blindly increasing the number of TEGs over the total heat providing area, called the occupancy ratio, does not always generate higher electricity, and there exists the optimal occupancy ratio for each condition of the system [14]. The physical configurations, such as the TEG installation position [15] and the heat exchanger height of the sandwich-plate exhaust system [16], are studied to increase the harvested power. Also, an optimization algorithm in the electrical configuration is proposed [17]. It optimizes the vast TEG array on the vehicle to fight spatial and temporal temperature locality problems and maximize the harvested power by array reconfiguration of serial and parallel connection among TEGs, depending on coolant flow rate and temperature.

Another way to increase TEG efficiency in system-level is to create a more significant temperature difference across a TEG. Since the heat source typically has a fixed condition, cooling a TEG cold side is the only way to increase the temperature difference. There are two different cooling methods to make temperature difference between each side of the TEG and they are classified into a natural convection cooling and a forced convection cooling. Natural convection cooling is a method that cools an object with a natural flow generated by density difference in the fluid occurring due to temperature gradients around a heat source, not by any external power. The natural convection cooling method applies widely in industrial fields, and usually has a heat sink on the top of it for better heat transfer. For the higher cooling capacity with the natural convection cooling, the heat sink shape and size are important factors for the cooling, so the optimal fin spacing [18] and the heat sink surface [19] are studied.

Different from the natural convection cooling, the forced convection cooling forces fluid to move for higher heat transfer by an external power, which is a pump or a fan. Since the forced convection is capable of not only increasing the net power, but also decreasing the net power, the relation between a coolant flow rate and the amount of harvested power has been studied for a TEG system with forced convection cooling [20]. In addition to the cooling system optimization, the researchers have investigated the advantages and disadvantages of natural convection cooling, forced convection cooling and combined forced-and-natural convection cooling [21,22].

The concept of thermoelectric self-cooling, which is cooling a TEG without external power consumption, is proposed [23]. The thermoelectric self-cooling system can increase the heat transfer rate that it interprets as the reduction of the convection thermal resistance between the air and the heat sink in the thermal equivalent circuit model. The reduced convection thermal resistance reduces the total thermal resistance of the system from the heat source to the air [24]. However, it can decrease the system net power harvested by a TEG system if the operating condition is not optimized. Since the coolant flow rate is the simple parameter but an essential parameter to control in the system, the coolant flow rate is optimized for the highest system net power [25]. A numerical methodology is developed and validated for the steady and transient thermal and electrical simulation for a self-cooling TEG with forced convection cooling, and a parametric study is done to find the effect of heat sink geometry for the maximum net power [26]. However, these self-cooling systems do not consider the most rational number of TEGs for the most efficient system net power, which let us also bring the concept of airflow recycling.

Computational fluid dynamics (CFD) computes numerical analysis and solves the complex heat transfer and fluidic problems for parameters that are difficult to obtain, such as the exact temperature of interfaces, for the maximum system net power [27,28]. CFD is very widely used recently with hardware development. A three-dimensional thermoelectric generator dynamics solver is built to

describe flow, heat transfer, fuel combustion, and electricity conversion in detail [29]. A multi-scale simulation framework for thermoelectric generator systems allows an accurate and efficient prediction of electric and thermal performance at steady-state conditions [30]. Improving CFD by incorporating temperature-dependent material properties for TEG and conjugate heat transfer obtains more accurate simulation results for impingement cooling on TEG [31]. Y. Wang et al. cover the importance and effects of temperature uniformity in electricity generation and optimize the fin distribution, considering fin dimension, angle, and spacing, for the maximum electric power generation [32]. An advanced numerical method by integrating CFD and TEG in association with a heat sink model has been developed for harvesting the waste heat from the flue gas, and performances of a dual thermoelectric module and a single thermoelectric module are compared [33]. It studies the effect of aspect ratio and tilt angle of TEG in a vertical chimney with CFD simulation and results in increases by pitch rising and angle inclining [34].

In consideration that the TEG under its operating range generally generates much more electricity as the bigger temperature difference, the forced convection is more suitable for the TEG system for the higher system net power. Most of the previous researches about forced convection cooling and the TEG have a fan(s) on the top of a heat sink, which locates above the TEG, and some of the researches have the fan placed at the side of the heat sink. We designate the TEG systems with two different fan mount positions as a top-mounted fan (TMF) TEG system and a side-mounted fan (SMF) TEG system. We propose the SMF-TEG system that can reduce the cooling power consumption by reusing airflow. The SMF- and TMF-TEG system balances among the additional power gain from adding a TEG, a diminution of cooling capacity, and a fan power increment to maximize the system net power. To have the most effective SMF-TEG system, we derive the power model of TEG and the fan. Next, we model the TEG system, including a TEG, a heat sink, airflow, and fan, and provide a precise CFD simulation result, which gives a guideline for the cooling system setup.

On the other hand, it is necessary to estimate the accurate hot and cold side temperature of TEG to calculate TEG-harvested power. To calculate the hot and cold side temperature, many assumptions need to be made to reduce complexity, and the SMF system structure, in which the cold side is perpendicular to the airflow, makes the temperature calculation more complex. To reduce the complexity and obtain values that are difficult to get in real life, many pieces of research on TEG adopted a CFD simulation program, which computes numerical analysis to analyze and solve problems involving fluid flows [27,28].

In summary, the novel contributions of this paper are as follows:

- We propose a side-mounted fan (SMF) system, which reuses an airflow for the most efficient system net power.
- We find the most rational number of TEG and most effective fan speed of the SMF system that generates the most efficient system net power by exploring design spaces.
- We present that the SMF-TEG system outperforms the TMF-TEG system on the system net power basis.

The remainder of this paper is organized as follows. Section 2 provides how airflow reuse is useful to cool multiple TEGs. The power models and problem statements are presented in Section 3. Section 4 describes parameters that we use in 3D modeling and simulation. In Section 5, we quantitatively compare the SMF system with the TMF system and show the SMF system outperforms the TMF system. Finally, Section 6 concludes this paper.

## 2. A Self-Cooling TEG System and Net Power Calculation

### 2.1. Airflow Reuse in a Forced Convection Cooling

When cooling a TEG system with a fan and a heat sink, there are two possible ways for assembling a fan and a heat sink. One way is a TMF system that places a fan on the top of the heat sink, as shown

in Figure 1a, and the other way is an SMF system that locates a fan at the side of the heat sink, Figure 1b. The TMF system requires a fan in every certain number of TEG, usually one or multiple TEGs depending on the fan size. On the other hand, in the SMF system, the airflow generated by a fan flows through one or multiple heat sinks depending on the number of TEGs. The outlet air temperature of a preceding TEG is lower than the cold side temperatures of following TEGs as long as the initial air temperature is lower than a hot side temperature. It enables us to create enough temperature difference on the following TEG and results in electricity generation.

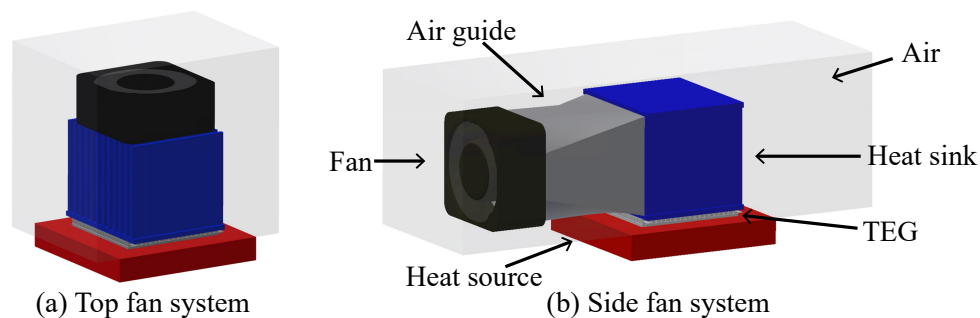


**Figure 1.** Thermoelectric generator (TEG) system with two different fan locations with part indication; (a) top-mounted fan (TMF) (baseline) and (b) side-mounted fan (SMF).

Figure 2 shows the results of a motivational example. We simulate the SMF system and the TMF system with one and three TEGs, and the air flows from left to right for the SMF system. The temperature of the heat source and the air is set at 200 and 25 °C, respectively. For the systems with one TEG, the SMF system has lower cold side temperature than the TMF system does, but, for three TEGs, the TMF system has lower cold side temperature. Also, in the SMF system with three TEGs, we can find the one SMF can also cool the second and the third TEG cold side temperature enough to generate electricity when the hot side temperature results between 192 and 198 °C. The first TEGs in each SMF system in Figure 2 have different cold side temperatures, which provides predictable information that the more number of TEGs, the less power harvested by TEG at the same TEG generation location. The total electricity generation from the SMF system may be smaller than that of the TMF system, but the system net power of the SMF system can be higher than that of the TMF system at the same number of TEGs and each most effective fan speed due to the total fan power consumption of each system. Here, we see the possibility of airflow reuse when we adopt an SMF system while a TMF system is not able to reuse airflow due to its structure. Thus we will reuse airflow from a single SMF and compare its system net power with a system net power of a TMF system. Then we will find the most effective fan speed and especially the number of TEGs for an SMF system to generate the most efficient system net power.

## 2.2. Net Power of a Self-Cooling TEG System

The system net power of a TEG system with a self-cooling  $P_{\text{Net}}$  can be declared as follows

$$P_{\text{Net}} = P_{\text{TEG}} - P_{\text{Fan}}, \quad (1)$$

where  $P_{\text{TEG}}$  and  $P_{\text{Fan}}$  denote a TEG-harvested power and cooling fan power consumption, respectively. As Equation (1) describes, a forced convection cooling can sometimes lead to a negative system net power with an unoptimized operation structure. In other words, the power consumption for a cooling and the TEG-harvested power have a trade-off relationship in the forced convection cooling system. Therefore, the operating condition of the cooling system should be finely tuned.

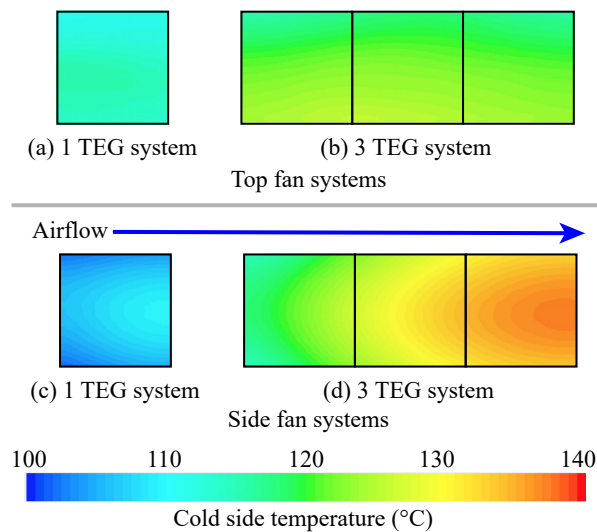


**Figure 2.** Cold side temperature of the TMF and SMF systems with one and three TEGs at a fan speed of 16,000 RPM; (a) 1 TEG system with one TMF, (b) 3 TEG system with three TMFs, (c) 1 TEG system with one SMF, and (d) 3 TEG system with one SMF.

### 2.3. Computational Fluid Dynamics Simulation

The calculation for the powers requires the values, such as the temperature of the TEG side plates, but it is not easy to measure their exact values in a real experiment. To obtain the exact values, we use a computational fluid dynamics (CFD) simulation program to estimate the values, such as the temperature of the TEG side plates, and control on surrounding conditions, such as ambient temperature and heat source temperature. A CFD simulation program is a general-purpose fluid flow simulation software that makes it possible to analyze turbulent and laminar flow problems, including heat transfer problems, in arbitrary geometries. It can simulate thermal, electrical, and fluidic problems with high reliability. A CFD simulation is widely used because it can control experiment conditions more precisely than an actual experiment and gives adequate results compared with a real test. With the CFD simulation, a user can easily build, set, control, implement, and achieve the target system and desired parameters, which are difficult in actual experiments. However, the CFD can result in incorrect or inaccurate simulation results and long computation times for various reasons, such as not enough convergence, inappropriate meshing, or too simple or complex models. A user needs to be aware of methods, such as proper convergence criteria with residuals and validation with the datasheet or the experimental data, to avoid the wrong simulation results. In this paper, we simulate a heat transfer phenomenon among a heat source, a TEG, a heat sink, and an airflow generated by a fan using a CFD program for accurate and under-control experiments. We use ‘Star-CCM+’ by SIEMENS, which is an accurate and reliable CFD simulation program popularly used in industries [35].

## 3. Optimizing Net Power of a Self-Cooling TEG System

### 3.1. Power Models

As we described in Section 2.2, the net power of the TEG system is calculated from the subtraction of fan power consumption from TEG-harvested power. For  $P_{TEG}$ , the current ( $I_{TEG}$ ) induced from a temperature difference across the TEG is denoted as follows [36]:

$$I_{TEG} = \frac{\alpha_M \cdot (T_{Hot} - T_{Cold})}{R_{Int} + R_{Load}}, \quad (2)$$

where  $\alpha_M$ ,  $T_{\text{Hot}}$ ,  $T_{\text{Cold}}$ ,  $R_{\text{Int}}$ , and  $R_{\text{Load}}$  are the Seebeck coefficients of a TEG module, a hot side temperature, a cold side temperature, an internal resistance of a TEG module, and a load resistance, respectively. The harvested power from TEG  $P_{\text{TEG}}$  is derived as follows:

$$P_{\text{TEG}} = I_{\text{TEG}}^2 \cdot R_{\text{Load}} = \left( \frac{\alpha_M \cdot (T_{\text{Hot}} - T_{\text{Cold}})}{R_{\text{Int}} + R_{\text{Load}}} \right)^2 \cdot R_{\text{Load}}, \quad (3)$$

Since the TEG-harvested power varies by the load resistance, we assume that the harvested power is extracted by a maximum power point tracking DC-DC converter. When a DC-DC converter operates at the maximum power point,  $R_{\text{Load}}$  matches  $R_{\text{Int}}$  by the maximum power transfer theorem. Thus,  $P_{\text{TEG}}$  becomes the maximum harvested power from TEG  $P_{\text{TEG,Max}}$  as follows [37]:

$$P_{\text{TEG,Max}} = \frac{\alpha_M^2 \cdot (T_{\text{Hot}} - T_{\text{Cold}})^2}{4 \cdot R_{\text{Int}}}. \quad (4)$$

We estimate  $\alpha_M$  and  $R_{\text{Int}}$  from the datasheet of a target TEG by a regression. We first attained the output power data and the resistance model at a matched load condition about both hot and cold side temperatures using the datasheet. Then, the Seebeck coefficient model is achieved by a curve-fitting with the obtained output power data, the achieved resistance model, and the maximum TEG-harvested power equation, Equation (4). The result regression model of the Seebeck coefficient  $\alpha_M$  and electrical resistance  $R_{\text{Int}}$  of the TEG module are as follows:

$$\begin{aligned} \alpha_M = & -2.0437 \times 10^{-7} \cdot T_{\text{Hot}}^2 + 1.3444 \times 10^{-7} \cdot T_{\text{Hot}} \cdot T_{\text{Cold}} + -2.0075 \times 10^{-7} \cdot T_{\text{Cold}}^2 \\ & + 1.2015 \times 10^{-4} \cdot T_{\text{Hot}} + 6.1784 \times 10^{-5} \cdot T_{\text{Cold}} + 0.0175. \end{aligned} \quad (5)$$

$$\begin{aligned} R_{\text{Int}} = & 1.911 \times 10^{-6} \cdot T_{\text{Cold}}^2 + 5 \times 10^{-6} \cdot T_{\text{Hot}} \cdot T_{\text{Cold}} \\ & + 8.044 \times 10^{-4} \cdot T_{\text{Hot}} + -4.75 \times 10^{-4} \cdot T_{\text{Cold}} + 0.3356. \end{aligned} \quad (6)$$

$T_{\text{Hot}}$  and  $T_{\text{Cold}}$  are considered in the regression models, Equations (5) and (6), because thermoelectric material properties vary with absolute values of both  $T_{\text{Hot}}$  and  $T_{\text{Cold}}$ , not only the temperature difference.  $T_{\text{Hot}}$  and  $T_{\text{Cold}}$  are difficult to estimate with a simple calculation, so are estimated from the CFD simulation.

Fan power consumption is proportional to the cube of the fan speed and calculated from affinity laws, which is also known as fan laws or pump laws, while a fan size is held constant in this paper. The affinity laws let engineers predict the pressure, flow rate, and power of the fan and the pump if two fans or pumps are dynamically similar. By the affinity laws, fan power consumption is calculated as follows:

$$P_{\text{Fan}} = \beta \cdot \omega^3, \quad (7)$$

where  $\beta$  is a ratio of the rated fan power to the cube of the rated fan speed. Fan speed  $\omega$  also directly affects the airflow rate and pressure, which affect  $T_{\text{Cold}}$ , as shown in Figure 3. We use the CFD simulation to calculate airflow rate and pressure, especially airflow through a heat sink. It is crucial to find the most effective fan speed to acquire the highest system net power of each system.

### 3.2. Problem Statement

The final goal of this work is maximizing the system net power of the TEG system by reusing airflow and finding the most effective fan speed and the most rational number of TEGs. Considering  $N$  TEG modules located in series, there are  $M_1, \dots, M_N$  modules. The SMF provides a possibility of recycling airflow after  $M_1$  module. The problem can be stated as below:

**Given:**

- TEG system composed of single SMF, TEG, heat sink, and heat source.
- Heating side temperature ( $T_{\text{Heat}}$ ) of the heat source.
- Ambient temperature.

**Control knob:**

- Fan speed ( $\omega$ ) and the number of TEGs ( $N$ ).

**Goal:**

- Find the most effective fan speed and the most rational number of TEGs ( $N$ ) producing the most efficient system net power ( $P_{\text{Net}}$ ) with a single SMF.

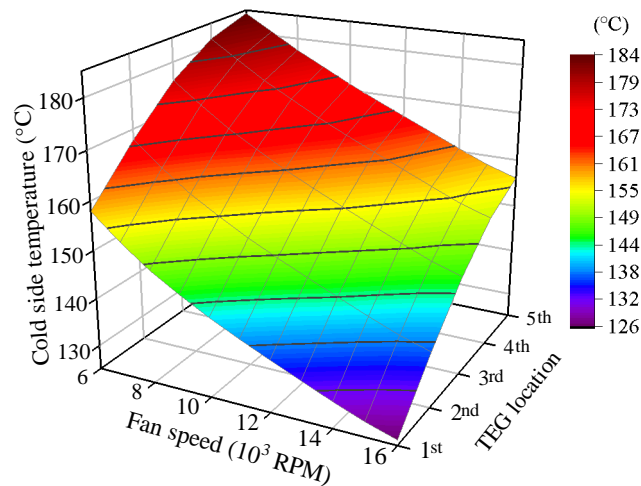


**Figure 3.** TEG cold side temperature at different locations according to fan speed in the five TEG system.

## 4. Modeling of a Self-Cooling TEG

### 4.1. TEG Modeling

For a reasonable and reliable TEG 3D model, we use a commercial TEG, TGM-199-1.4-0.8 (Kryotherm, St. Petersburg, Russia) [38], as shown in Figure 4a. The TEG model consists of electrical interconnects, electrical interconnect ends, pairs of thermoelectric elements, and side plates. All the thermoelectric elements in this model are connected in series except that the last two elements are connected in parallel at each electrical interconnect end. The total dimension of the TEG given in the datasheet is  $40 \times 40 \times 3.25$  mm (L  $\times$  W  $\times$  H). The detailed dimension of each part is important to calculate the amount of heat transfer correctly, but the manufacturer does not provide it in detail. Hence, we disassemble the TEG and measure the dimension of each part, as listed in Table 1. The 3D model of TEG used in a CFD simulation is presented in Figure 4b,c. Though the simulation complexity increases significantly, all the thermoelectric elements are modeled in detail for precise thermoelectric effect, Ohmic heating, and heat transfer.

The material property of the TEG component is essential for accurate simulation. Required properties for thermoelectricity phenomenon simulation are density, thermal conductivity, specific heat, the Seebeck coefficient, and electrical conductivity. The materials of each component and their property values are listed in Table 2. We model the power generation capacity of TEG using a datasheet. Figure 5 shows the amount of harvested power from TEG according to the hot side and cold

side temperature. The parameters of Equation (4) are extracted within the recommended operating temperature, from 0 to 200 °C.

**Table 1.** Dimensions of all components.

Part	Dimension (mm)			Q'ty
	L	W	H	
<b>TEG</b>	40	40	3.25	-
Thermoelectric element	1.5	1.5	0.75	400
Electrical interconnect	3.5	1.5	0.25	395
Electrical interconnect end	7.5	1.5	0.25	4
Side plate	40	40	1	2
<b>Heat sink</b>	48	40	42	1/TEG
Fin	2	40	0.75	12
Fin to fin	3	-	-	-
Top/bottom plate	48	40	2	2
<b>Fan</b>	40	20	40	1
<b>Heat source</b>	60	20 + 40 × TEG#	10	1

**Table 2.** Material properties for each component [35,39].

Part	Material	Density (g/cm <sup>3</sup> )	Thermal Cond. * (W/m·K)	Specific Heat (J/kg·K)	Electrical Cond. * (S/m)
<b>TEG</b>					
Thermoelectric element	Bismuth Telluride	7.53	1.5	544.28	-
Electrical interconnect	Copper	8.96	386.0	385.19	$5.96 \times 10^7$
Side plate	Alumina Ceramic	3.57	35.3	837.36	-
<b>Heat sink</b>	Aluminum	2.71	204.0	900.16	-
<b>Heat source</b>	Aluminum	2.71	204.0	900.16	-

\* abbreviation of conductivity.

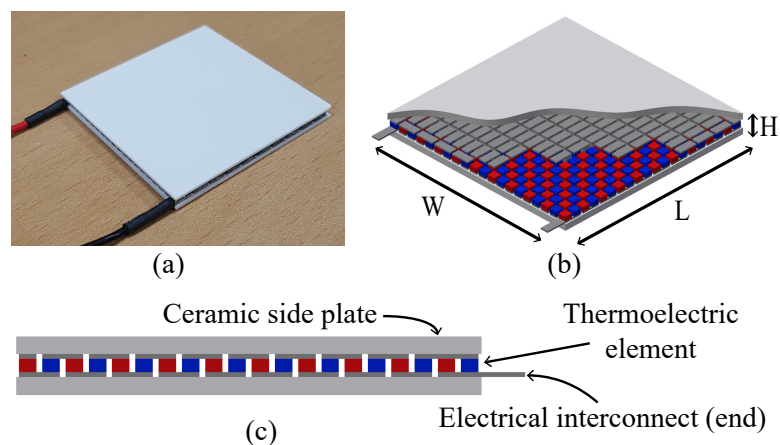


**Figure 4.** TGM-199-1.4-0.8 TEG and its 3D model; (a) picture of a target TEG, (b) isometric view of a target TEG 3D model, and (c) side view of a target TEG 3D model.

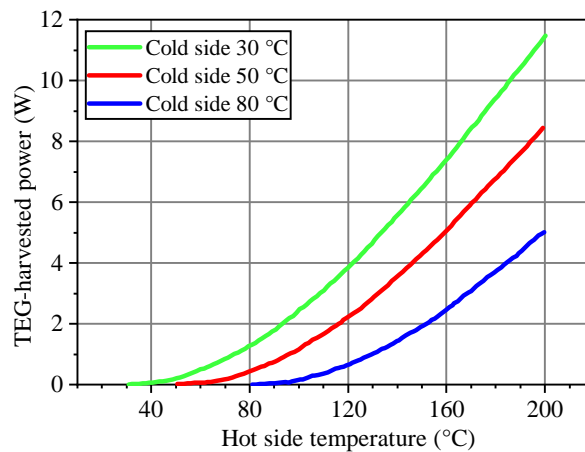


**Figure 5.** TEG-harvested power according to the hot side and cold side temperature [38].

#### 4.2. Cooling System Modeling

The target system has a forced convection cooling system composed of ambient air, a fan, and a heat sink. A fan creates airflow cooling a cold side of a TEG while a heat sink helps a heat transfer from the cold side of the TEG to the coolant air, which is an ambient air in this work. We select a commercial fan, 9GA0412P6G001 (Sanyo Denki, Tokyo, Japan) [40] as shown in Figure 6a–c. Figure 6d,e show the manually designed heat sinks, and their dimensions are listed in Table 1.

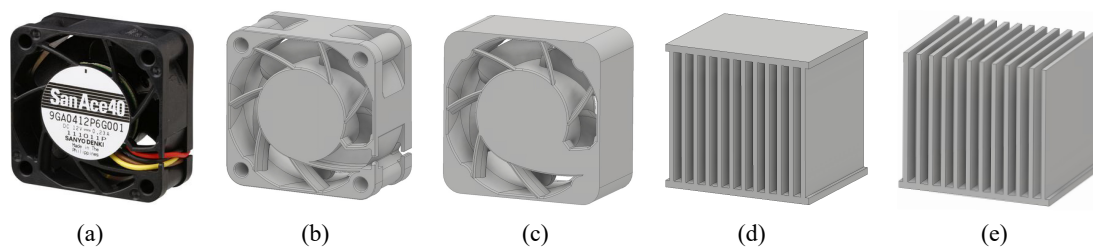


**Figure 6.** A commercial fan, Sanyo Denki 9GA0412P6G001, and a manually designed heat sink; (a) a commercial fan, (b) a detailed 3D fan model from the manufacturer, (c) a simplified 3D fan model for the simulation, (d) a 3D heat sink model for the side fan system, and (e) a 3D heat sink model for the TMF system.

The shape of a fan in the 3D model is essential because it affects the airflow generated by a fan, and a small defect in the 3D model can result in the wrong simulation. Thus, we start a fan modeling from a detailed 3D model provided by the manufacturer to minimize possible errors, but the detailed 3D model increases the computation time, which is a drawback of CFD simulation. To alleviate a long computation time and complexity, we simplify the fan's outer frame, which does not affect the airflow. However, the details of the inner shape, such as the hub and the blades, remain unchanged, which directly influences the cooling performance.

The amount of power consumed by a fan affects the system net power, so the correct power consumption model of a fan is necessary. The target fan, 9GA0412P6G001, has the rated power consumption 2.76 W at the rated rotation speed, 16,000 RPM. The maximum airflow and the maximum static pressure at the rated power are  $0.42 \text{ m}^3/\text{min}$  and 318 Pa, respectively. We extract  $\beta$  from the datasheet of the fan and calculate the fan power consumption using Equation (7). The CFD program automatically considers airflow and static pressure during its simulation.

Another component of a cooling system is a heat sink. We design two heat sinks for an SMF system and a TMF system. The only difference between the two types of heat sinks is that a heat sink for an SMF system has a top plate for better airflow recycling, as shown in Figure 6d,e. The top plate is

necessary for the SMF system to create the airflow straight and extensive contacts between the coolant air and the surface of the heat sink, which enhances a heat transfer from the TEG. If the top plate does not exist in the SMF system, airflow starts to flow in the upper direction due to its high pressure build-up behind, resulting in inadequate cooling in the behind portion of the heat sink.

#### 4.3. Assembled TEG System Modeling

Before the simulation, all the components are put together as a TEG system. The basic assembled target system used in the CFD simulation is shown in Figure 1. We first model a TMF system as a baseline. The heat source locates at the bottom, and the TEG and heat sink stack on top of a heat source. Lastly, a cooling fan is installed on the top of the heat sink. In a fan structure, connecting bridges between the hub and the frame, as shown in Figure 6a–c, create different air velocity and stream over the fan outlet section. Thus, the airflow guide is necessary for evenly distributed airflow before entering heat sinks. However, the airflow guide is not applied in the TMF system because the temperature of the TEG cold side is evenly distributed well without the airflow guide. We assume that there is no heat transfer through the fan and the airflow guide in the simulation. The SMF- and TMF-TEG systems for the simulation are designed with one to five TEGs to ensure that we find the most efficient system net power. Total computational components and boundary conditions are shown in Figure 7.

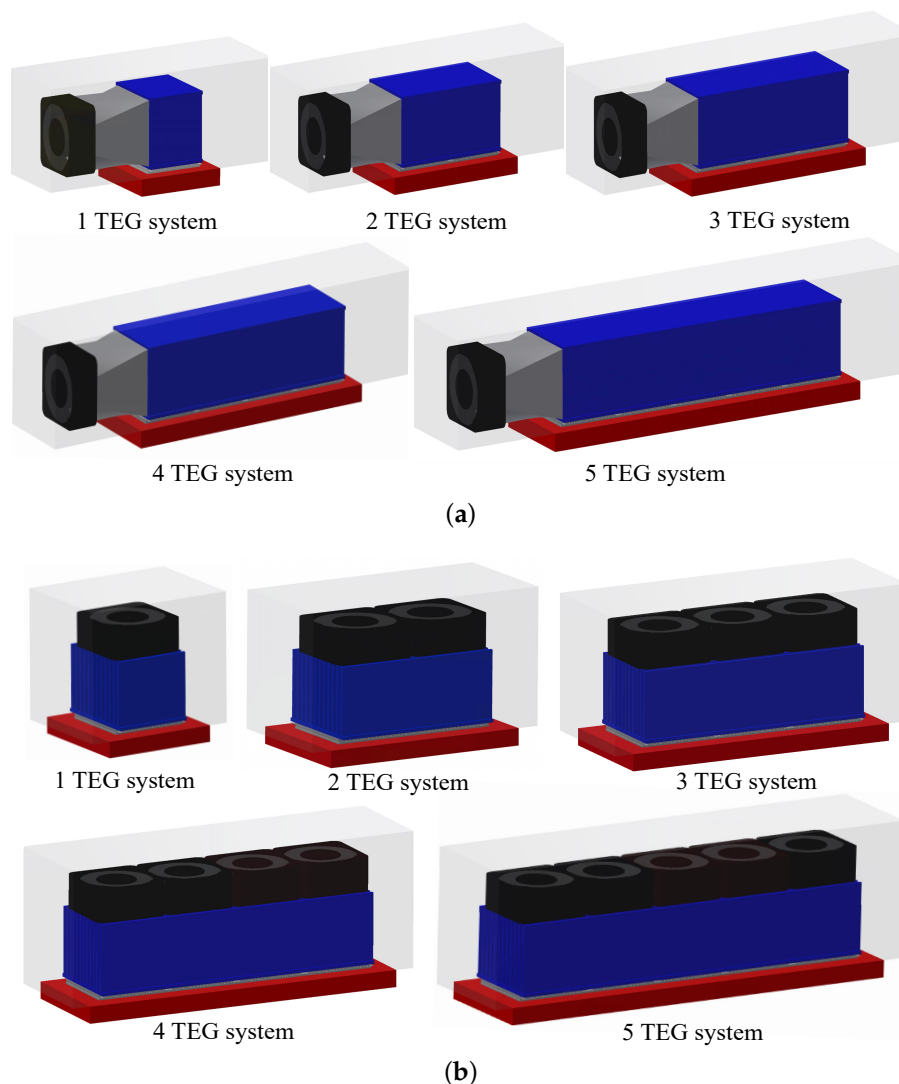


**Figure 7.** SMF and TMF systems; (a) SMF-TEG systems (Proposed system) and (b) TMF-TEG systems.

Thermal contact resistance is one of the important factors for the correct result with the assembly. In a real experiment, interfacing surfaces among components are not perfectly smooth, and these imperfectly smooth interfaces create air gaps that reduce the heat transfer rate between interfacing surfaces. We regard the reduced heat transfer rate as an increase in the thermal contact resistance to execute CFD simulation. The thermal interface material (TIM) and the proper pressure are applied to reduce the thermal contact resistance between the contact surfaces because the pressure reduces the air gap sizes, and the TIM with the high thermal conductivity, from 0.9 to 20 W/m-K [41] depending on the materials, fills the air gap that has a lower thermal conductivity of about 0.026 W/m-K [42]. However, when modeling the TIM, its real size is too minimal ( $\mu\text{m}$ ) compared with that of other parts (mm), and such a small 3D model can increase the possibility of an error. In the simulation, instead of embodying and applying the thermal contact material as a 3D model, we input a contact thermal contact resistance value. The thermal contact resistance value is  $1.7 \times 10^{-5} \text{ m}^2\text{-K/W}$  from [41] for every interfacing surface between each TEG hot side and the heat source and between each TEG cold side and the heat sink.

## 5. Experiment

### 5.1. Experimental Setup

After modeling components, setting up for correct meshing models, physics models, and boundary conditions are essential to run the simulation. The simulation performs in a steady-state and three-dimensional simulation and uses the segregated solver. Ideal gas is applied to air. Thermoelectric and electrical interconnect parts include thermoelectricity and ohmic heating.

For the meshing, the base mesh size is 7 mm, and the minimum base size is 0.21 mm, which is 3% of the base mesh size. Degrees of freedom (DOFs) is zero in our system because we set the fan to rotate at the input fan speed. We used surface remesher and automatic surface repair to optimize the quality of the surface and correct a range of geometric type problems. Polyhedral mesh has several benefits over other types of mesh; each cell has more interfacing neighbors so that gradients can be much better approximated compared with tetrahedral mesh [43]. Comparison among polyhedral, tetrahedral, and hexahedral mesh types is made, and it shows that polyhedral mesh converges faster and has fewer cells than for the same geometry [44]. Thin mesher is applied to generate a prismatic type volume mesh for thin volumes and improves overall cell quality. Prism layer mesh is used to generate orthogonal prismatic cells next to wall surfaces or boundaries and is necessary to improve the accuracy of the flow solution. The total number of cells is, for example, 9,711,444 cells for 1 TEG system with SMF. One TEG is composed of thermoelectric elements with 644,000 cells, side plates with 588,000 cells, and electrical interconnects with 552,000 cells approximately. Mesh quality is checked and confirmed according to the proposed method in the CFD program manual, and Figures 8 and 9 show meshes of each component.

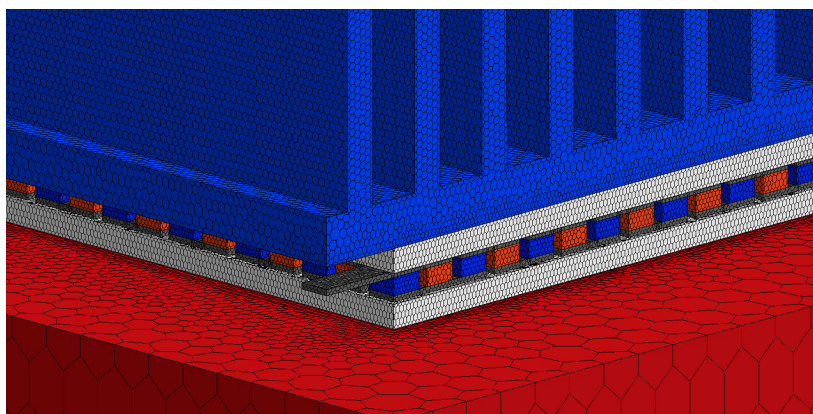
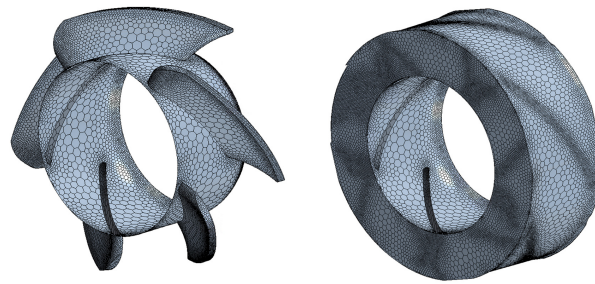


Figure 8. Mesh grid of the TEG system.



**Figure 9.** Mesh grid of the fan blades (left) and the total rotating region (right).

After the mesh generation, we set the boundary and initial condition values. We set the bottom of the heat source, not a whole heat source, at a specific temperature of 200 °C. It is set to reflect the real condition, in which a contact surface between a heat source and an object is not constant if there exists a temperature difference between two objects. Ambient air temperature is set at a room temperature of 25 °C. We assume that the bottom side temperature of the heat source and the air is set at a fixed value of 200 and 25 °C, respectively. The typical TEG system is applied to such hot steam or petrochemical pipes in power or petrochemical plants. The fluids in the pipes have enough high temperature and fast flow rate [45,46], so we can regard the transferred heat power is enough, which enables us to make such an assumption as a fixed temperature of the heat source bottom side. The air 3D model has all the sides, except the bottom side contacting the heat source, open for air circulation, which means air can flow in and out of the system according to the airflow.

The fan blades and hub are designed and set to rotate in the simulation, instead of a simple inlet flow from the boundary surface. We use, for the rotation of the blades, a moving reference frame concept, which the CFD program recommends for a steady-state simulation. Fan speed is an important factor in determining the system net power of the TEG system. We simulate the TEG system for fan speed ranging from 6000 to 16,000 RPM, in increments of 1000 RPM. Note that we select the fan speed range and increment for simulation after the test simulation to reduce the design exploration space. The baseline for comparison is a TEG system with a fan located on top of the TEG. The proposed TEG system has a single fan at the side of the TEG, which can cool several TEGs by reusing airflow at the same time. We simulate the proposed TEG system with the number of TEGs from one to five to find the most rational number of TEGs, producing the most efficient  $P_{Net}$  with a single SMF. We also find the most effective fan speed for each system. Note that for our CFD model validation, we confirmed the same output power from the simulation result and the datasheet by setting the air temperature and fan speed to achieve the hot and cold side temperatures provided in the datasheet.

## 5.2. Experimental Result

First, with a single TEG, a heat sink, and a fan, the SMF-TEG system outperforms the TMF-TEG system. Figure 10 shows the system's net power of all the SMF systems comparing with that of a TMF system, comprising one TEG and one fan as a baseline. Note that we select simulation results at five different fan speeds of each system, and the most efficient system net power point is located in the middle. TEG systems with an SMF generate more system net power than the baseline system for all of the fan speed.

Second, with more TEGs, an SMF system can generate more power while the number of fans remains one. In Figure 10, the system net power of the SMF system increases up to four TEGs comparing with the baseline system, which is a TMF system with one TEG and one cooling fan. The SMF system can cool the several TEGs by reusing airflow from a single fan. Therefore, the most efficient system net power increases up to the system with four TEGs at the cost of higher fan power.

After that, the most efficient system net power generated by the SMF TEG system decreases. Hence, we compare the SMF system generating more system net power to the TMF system with the same number of TEGs even though the SMF system has a smaller cooling fan. In Figure 11, we compare

the TMF-TEG system and SMF-TEG system, which have three TEGs. Note that the TMF system uses the same number of fans as the number of TEGs, so three fans in this case. The SMF system with three TEGs generates the electricity of 1.906 W at 12,000 RPM while the TMF system generates the system net power of 1.825 W at 8000 RPM even though the SMF system consumes more total fan power to cool TEGs. Therefore, the SMF system is able to generate 4.43% higher power than the TMF system with the same three TEGs.

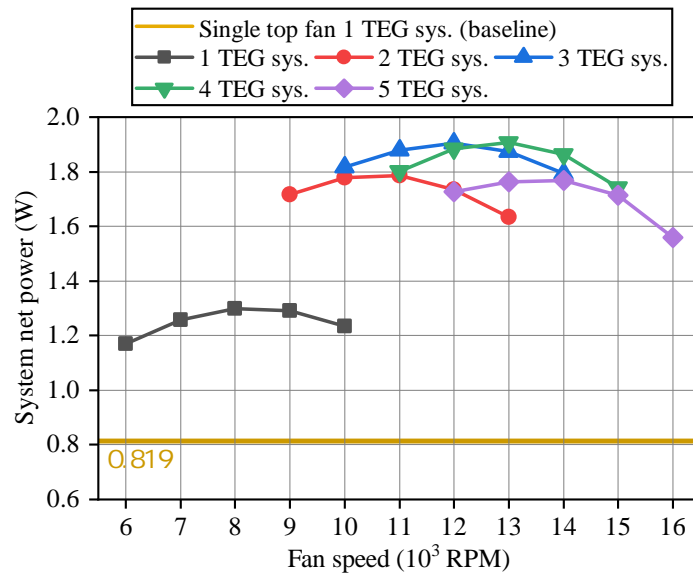


**Figure 10.** System net power of the various SMF systems at different fan speeds compared with the most efficient system net power of the TMF system with one TEG.

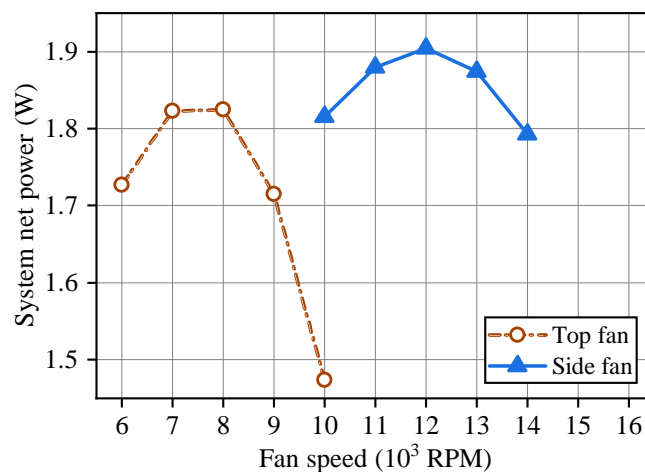


**Figure 11.** System net power comparison between the TMF system with three TEGs and three fans and the SMF systems with three TEGs and a single fan.

An SMF system with more TEGs requires a higher fan speed to make more airflow shown in Figure 10. However, the air temperature still increases, and the fan power increase may exceed the generated power from additional TEGs. We confirm it with the cold side temperature distribution on the TEGs at their most effective fan speed, as shown in Figure 12. Note that the hot side temperature of all the systems is between 193 and 198 °C, so the effect of the hot side temperature is not noticeable. The cold side temperature of each TEG rises as the number of TEGs increase even though the most effective fan speed increases.

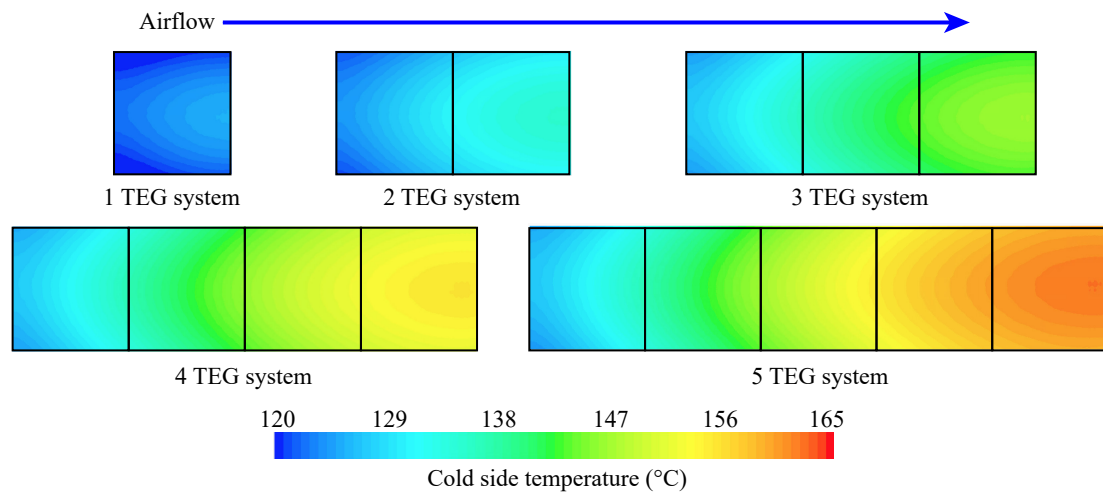


**Figure 12.** TEG cold side temperature distribution of all the SMF systems at their most effective fan speeds. The hot side temperature of all the systems is between 193 and 198 °C.

Figure 13 shows the temperature field of heat sinks at their most effective fan speeds. It shows that heat sinks in the TEG system with fewer TEGs have a colder temperature. Figure 14 shows the TEG-harvested power, total fan power, and system net power of different configurations at their most effective fan speed. For the SMF system, it generates more system net power than the TMF system by reusing airflow effectively up to four TEGs. The harvested power increment diminishes faster because reusing airflow makes the air temperature high and, in turn, reduces cooling capability. The SMF system consumes more fan power to make a faster airflow, but the power harvested by additional TEG becomes smaller as the number of TEGs in the SMF system increases. Also, the harvested power by each TEGs at the same location in different configurations become lower as the number of TEGs increase, but they converge. We confirm this by analyzing the generated power from each TEG, as shown in Figure 15.

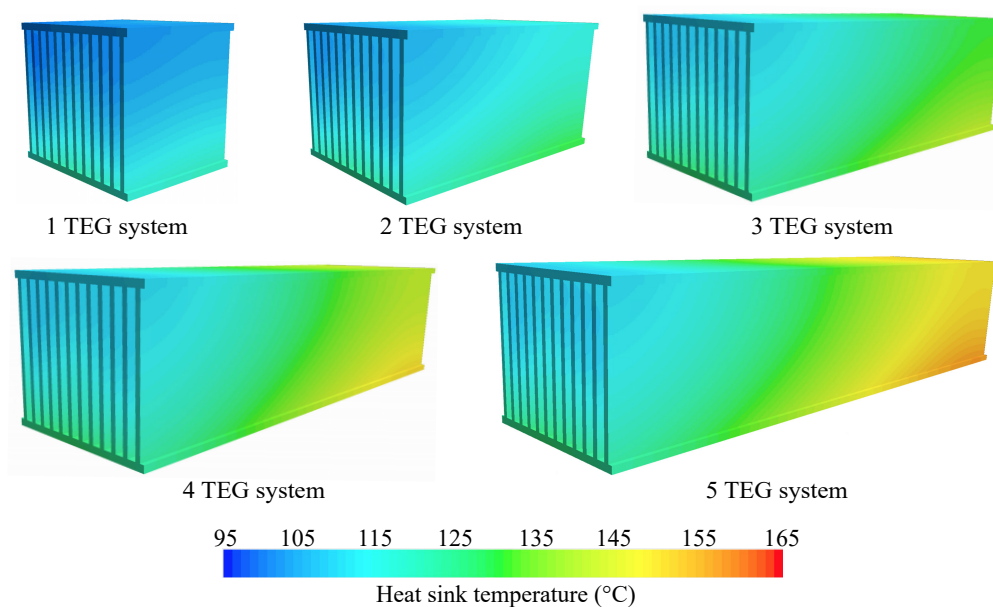


**Figure 13.** Temperature distribution of heat sinks at the most effective fan speed of SMF systems.

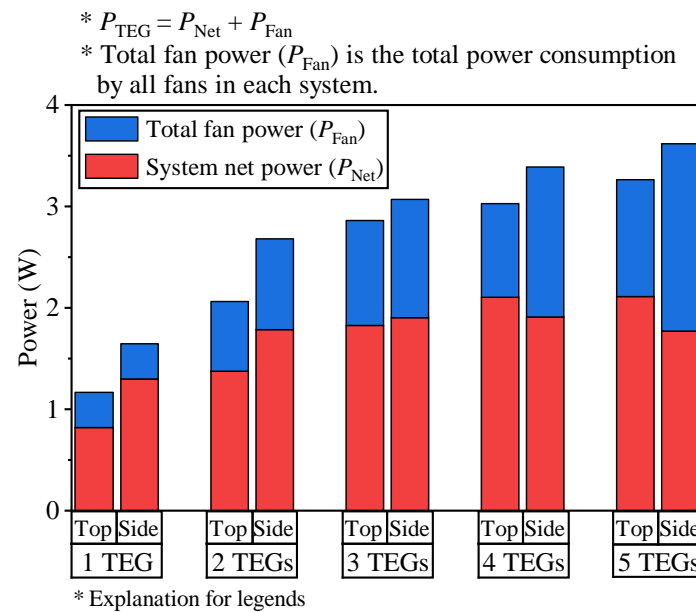


**Figure 14.** TEG-harvested power consisted of the system net power and the total fan power in all the systems at their system net power.

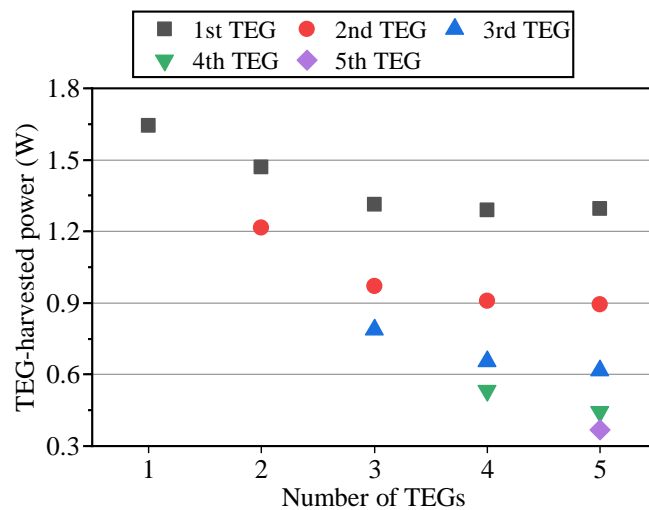


**Figure 15.** Each TEG-harvested power in all the SMF systems at their most efficient system net power.

Table 3 summarizes the most effective fan speed, the system net power, and the average net power per unit TEG for each system configuration. The most effective fan speed of the TMF system does not change as the number of TEG increases while the most effective fan speed of the SMF system increases as the number of TEG increases. The increase in the fan power consumption due to the higher fan speed and the limited heat exchange capacity are the main reasons for lower net power per unit TEG with a higher number of TEGs. However, the SMF system generates up to 58.6% more average net power per unit TEG compared to the TMF system with the same number of TEGs. We find that the SMF system generates the most efficient  $P_{Net}$  at 13,000 RPM with four TEGs.

**Table 3.** Summary table of the most effective fan speed, the average net power per unit TEG, and the most efficient system net power according to the different TEG configurations.

Number of Fans (Q'ty)	Number of TEGs (Q'ty)	Most Effective Fan Speed (RPM)	Fan Power Consumption (W)	Most Efficient System Net Power (W)	Average Net Power per Unit TEG (W/TEG)
<b>TMF</b>					
1	1	8000	0.345	0.819	0.819
2	2	8000	0.345	1.373	0.687
3	3	8000	0.345	1.825	0.608
4	4	7000	0.231	2.106	0.527
5	5	7000	0.231	2.109	0.422
<b>SMF</b>					
1	1	8000	0.345	1.299	1.299
1	2	11,000	0.897	1.785	0.893
1	3	12,000	1.164	1.906	0.635
1	4	13,000	1.48	1.907	0.477
1	5	14,000	1.849	1.768	0.354

## 6. Conclusions

A TEG is a promising energy harvester that generates electricity from waste heat. The amount of harvested electricity from the TEG depends on the temperature difference between the hot side and the cold side of a TEG. Therefore, a cooling system and its power consumption determine the amount of system net power from a TEG system.

In a forced convection cooling with air, the total fan power consumption of the system can be reduced by placing a fan at the side of the heat sink and reusing the airflow. However, airflow reuse diminishes cooling capability. Hence, we found the most rational number of TEGs and the most effective fan speed producing the most efficient system net power in the SMF systems with a various number of TEGs. We modeled a commercial fan and TEG with the provided material property by the manufacturer and specific dimensions that we manually measured. We then used the CFD simulation program, which is reliable and commonly used in industries, to calculate the accurate temperature and harvested power. The TEG-harvested power was estimated with the Seebeck coefficient, internal electrical resistance, and the fan power consumption calculated with the affinity laws. The Seebeck coefficient and internal resistance values were obtained from our regression model. We found that the SMF system with four TEGs generates the most efficient system net power of 1.907 W at 13,000 RPM, which is the most among all the SMF systems. The SMF system with up to three TEGs harvests more system net power than the TMF system with the extra benefit of reducing the fan cost. Compared with the baseline, which has the same number of the TEG and TMFs and dominantly used in academic researches, the SMF system with one TEG generates a higher system net power of 58.6% than the TMF system with one TEG.

**Author Contributions:** Conceptualization, J.K. and Y.H.C.; methodology, J.K.; software, Y.H.C.; validation, J.P., N.C. and J.K.; formal analysis, N.C.; investigation, Y.H.C.; resources, N.C.; data curation, J.P.; writing—original draft preparation, Y.H.C.; writing—review and editing, J.K.; visualization, J.P.; supervision, J.K.; project administration, N.C.; funding acquisition, N.C. All authors have read and agreed to the published version of the manuscript.

**Funding:** This work was supported by the National Research Foundation of Korea (NRF) Grant funded by the Korean Government (MSIP) (NRF-2015R1A5A1036133), (MSIT) (Nos. NRF-2018R1C1B5047150 and NRF-2019R1F1A1060525).

**Conflicts of Interest:** The authors declare no conflict of interest.

## References

- Saha, B.; Perez-Taborda, J.A.; Bahk, J.H.; Koh, Y.R.; Shakouri, A.; Martin-Gonzalez, M.; Sands, T.D. Temperature-dependent thermal and thermoelectric properties of n-type and p-type Sc<sub>1-x</sub>Mg<sub>x</sub>N. *Phys. Rev. B* **2018**, *97*, 085301. [\[CrossRef\]](#)
- Lee, J.; Kim, S.; Marconnet, A.; in't Zandt, M.; Asheghi, M.; Wong, H.S.P.P.; Goodson, K.E. Thermoelectric characterization and power generation using a silicon-on-insulator substrate. *J. Microelectromech. Syst.* **2011**, *21*, 4–6. [\[CrossRef\]](#)
- O'Dwyer, C.; Chen, R.; He, J.H.; Lee, J.; Razeeb, K.M. Scientific and Technical Challenges in Thermal Transport and Thermoelectric Materials and Devices. *ECS J. Solid State Sci. Technol.* **2017**, *6*, N3058–N3064. [\[CrossRef\]](#)
- Shaikh, F.K.; Zeadally, S. Energy harvesting in wireless sensor networks: A comprehensive review. *Renew. Sustain. Energy Rev.* **2016**, *55*, 1041–1054. [\[CrossRef\]](#)
- Zhao, L.D.; Chang, C.; Tan, G.; Kanatzidis, M.G. SnSe: A remarkable new thermoelectric material. *Energy Environ. Sci.* **2016**, *9*, 3044–3060. [\[CrossRef\]](#)
- Sun, L.; Jiang, P.; Liu, H.; Fan, D.; Liang, J.; Wei, J.; Cheng, L.; Zhang, J.; Shi, R. Graphdiyne: A two-dimensional thermoelectric material with high figure of merit. *Carbon* **2015**, *90*, 255–259. [\[CrossRef\]](#)
- Kim, S.I.; Lee, K.H.; Mun, H.A.; Kim, H.S.; Hwang, S.W.; Roh, J.W.; Yang, D.J.; Shin, W.H.; Li, X.S.; Lee, Y.H.; et al. Dense dislocation arrays embedded in grain boundaries for high-performance bulk thermoelectrics. *Science* **2015**, *348*, 109–114. [\[CrossRef\]](#)
- Hu, L.; Zhu, T.; Liu, X.; Zhao, X. Point defect engineering of high-performance Bismuth-Telluride-based thermoelectric materials. *Adv. Funct. Mater.* **2014**, *24*, 5211–5218. [\[CrossRef\]](#)
- Hsiao, Y.; Chang, W.; Chen, S. A mathematic model of thermoelectric module with applications on waste heat recovery from automobile engine. *Energy* **2010**, *35*, 1447–1454. [\[CrossRef\]](#)
- He, W.; Wang, S.; Lu, C.; Zhang, X.; Li, Y. Influence of different cooling methods on thermoelectric performance of an engine exhaust gas waste heat recovery system. *Appl. Energy* **2016**, *162*, 1251–1258. [\[CrossRef\]](#)
- Orr, B.; Akbarzadeh, A.; Mochizuki, M.; Singh, R. A review of car waste heat recovery systems utilising thermoelectric generators and heat pipes. *Appl. Therm. Eng.* **2016**, *101*, 490–495. [\[CrossRef\]](#)
- Özdemir, A.E.; Köysal, Y.; Özbaş, E.; Atalay, T. The experimental design of solar heating thermoelectric generator with wind cooling chimney. *Energy Convers. Manag.* **2015**, *98*, 127–133. [\[CrossRef\]](#)
- Kim, S.J.; We, J.H.; Cho, B.J. A wearable thermoelectric generator fabricated on a glass fabric. *Energy Environ. Sci.* **2014**, *7*, 1959–1965. [\[CrossRef\]](#)
- Aranguren, P.; Astrain, D.; Rodríguez, A.; Martínez, A. Net thermoelectric power generation improvement through heat transfer optimization. *Appl. Therm. Eng.* **2017**, *120*, 496–505. [\[CrossRef\]](#)
- Eldesoukey, A.; Hassan, H. 3D model of thermoelectric generator (TEG) case study: Effect of flow regime on the TEG performance. *Energy Convers. Manag.* **2019**, *180*, 231–239. [\[CrossRef\]](#)
- He, W.; Wang, S.; Yue, L. High net power output analysis with changes in exhaust temperature in a thermoelectric generator system. *Appl. Energy* **2017**, *196*, 259–267. [\[CrossRef\]](#)
- Kim, J.; Baek, D.; Ding, C.; Lin, S.; Shin, D.; Lin, X.; Wang, Y.; Cho, Y.H.; Park, S.H.; Chang, N. Dynamic Reconfiguration of Thermoelectric Generators for Vehicle Radiators Energy Harvesting Under Location-Dependent Temperature Variations. *IEEE Trans. Very Large Scale Integr. (VLSI) Syst.* **2018**, *26*, 1241–1253, doi:10.1109/TVLSI.2018.2812705. [\[CrossRef\]](#)
- Wang, C.C.; Hung, C.I.; Chen, W.H. Design of heat sink for improving the performance of thermoelectric generator using two-stage optimization. *Energy* **2012**, *39*, 236–245. [\[CrossRef\]](#)
- Gou, X.; Xiao, H.; Yang, S. Modeling, experimental study and optimization on low-temperature waste heat thermoelectric generator system. *Appl. Energy* **2010**, *87*, 3131–3136. [\[CrossRef\]](#)
- Rezania, A.; Rosendahl, L.; Andreasen, S.J. Experimental investigation of thermoelectric power generation versus coolant pumping power in a microchannel heat sink. *Int. Commun. Heat Mass Transf.* **2012**, *39*, 1054–1058. [\[CrossRef\]](#)
- Kobus, C.; Oshio, T. Development of a theoretical model for predicting the thermal performance characteristics of a vertical pin-fin array heat sink under combined forced and natural convection with impinging flow. *Int. J. Heat Mass Transf.* **2005**, *48*, 1053–1063. [\[CrossRef\]](#)
- Lv, S.; He, W.; Jiang, Q.; Hu, Z.; Liu, X.; Chen, H.; Liu, M. Study of different heat exchange technologies influence on the performance of thermoelectric generators. *Energy Convers. Manag.* **2018**, *156*, 167–177. [\[CrossRef\]](#)

23. Martínez, A.; Astrain, D.; Rodríguez, A. Experimental and analytical study on thermoelectric self cooling of devices. *Energy* **2011**, *36*, 5250–5260. [[CrossRef](#)]
24. Moran, M.J.; Shapiro, H.N.; Munson, B.R.; DeWitt, D.P. *Introduction to Thermal Systems Engineering: Thermodynamics, Fluid Mechanics, and Heat Transfer*; John Wiley & Sons, Inc.: Hoboken, NJ, USA, 2003; pp. 359–404.
25. Kiflemariam, R.; Lin, C.X. Numerical simulation of integrated liquid cooling and thermoelectric generation for self-cooling of electronic devices. *Int. J. Therm. Sci.* **2015**, *94*, 193–203. [[CrossRef](#)]
26. Lin, C.X.; Kiflemariam, R. Numerical Simulation and Validation of Thermoelectric Generator Based Self-Cooling System with Airflow. *Energies* **2019**, *12*, 4052. [[CrossRef](#)]
27. Lakhkar, N.; Hossain, M.; Agonafer, D. CFD modeling of a thermoelectric device for electronics cooling applications. In Proceedings of the 2008 11th Intersociety Conference on Thermal and Thermomechanical Phenomena in Electronic Systems, Orlando, FL, USA, 28–31 May 2008; pp. 889–895.
28. Fernández-Yañez, P.; Armas, O.; Capetillo, A.; Martínez-Martínez, S. Thermal analysis of a thermoelectric generator for light-duty diesel engines. *Appl. Energy* **2018**, *226*, 690–702. [[CrossRef](#)]
29. Shen, R.; Gou, X.; Zhong, J. A Three-dimensional Dynamic Analysis CFD Tool for Thermoelectric Generators. *Int. J. Thermophys.* **2020**, *41*, 20. [[CrossRef](#)]
30. Höglblom, O.; Andersson, R. A simulation framework for prediction of thermoelectric generator system performance. *Appl. Energy* **2016**, *180*, 472–482. [[CrossRef](#)]
31. Pfeiffelmann, B.; Benim, A.C.; Joos, F. Computational Investigation of Impingement Cooling of Thermoelectric Generators. *Heat Transf. Eng.* **2019**, 1–14, doi:10.1080/01457632.2019.1699296.
32. Wang, Y.; Wu, C.; Tang, Z.; Yang, X.; Deng, Y.; Su, C. Optimization of fin distribution to improve the temperature uniformity of a heat exchanger in a thermoelectric generator. *J. Electron. Mater.* **2015**, *44*, 1724–1732. [[CrossRef](#)]
33. Chen, W.H.; Lin, Y.X.; Chiou, Y.B.; Lin, Y.L.; Wang, X.D. A computational fluid dynamics (CFD) approach of thermoelectric generator (TEG) for power generation. *Appl. Therm. Eng.* **2020**, *173*, 115203. [[CrossRef](#)]
34. Khalil, H.; Hassan, H. 3D study of the impact of aspect ratio and tilt angle on the thermoelectric generator power for waste heat recovery from a chimney. *J. Power Sources* **2019**, *418*, 98–111. [[CrossRef](#)]
35. Star-CCM+. SIEMENS Star-CCM+ Homepage. Available online: <https://www.plm.automation.siemens.com/global/ko/products/simcenter/STAR-CCM.html> (accessed on 17 June 2020).
36. Chen, W.H.; Wu, P.H.; Wang, X.D.; Lin, Y.L. Power output and efficiency of a thermoelectric generator under temperature control. *Energy Convers. Manag.* **2016**, *127*, 404–415. [[CrossRef](#)]
37. Yan, Y.; Malen, J.A. Periodic heating amplifies the efficiency of thermoelectric energy conversion. *Energy Environ. Sci.* **2013**, *6*, 1267–1273. [[CrossRef](#)]
38. Kryotherm. Specification of Generating Thermoelectric Modules TGM-199-1.4-0.8. Available online: <http://kryothermtec.com/assets/dir2attz/ru/TGM-199-1.4-0.8.pdf> (accessed on 17 June 2020).
39. Ferrotec USA. Thermoelectric Technical Reference. Available online: <https://thermal.ferrotec.com/technology/thermoelectric-reference-guide/thermalRef02/> (accessed on 17 June 2020).
40. Sanyo Denki. Cooling Fan San Ace. Available online: [https://www.sanyodenki.com/archive/document/product/cooling/catalog\\_E\\_pdf/San\\_Ace\\_E.pdf](https://www.sanyodenki.com/archive/document/product/cooling/catalog_E_pdf/San_Ace_E.pdf) (accessed on 17 June 2020).
41. Sarvar, F.; Whalley, D.C.; Conway, P.P. Thermal interface materials-A review of the state of the art. In Proceedings of the 2006 1st Electronic Systemintegration Technology Conference, Dresden, Germany, 5–7 September 2006; Volume 2, pp. 1292–1302.
42. Lemmon, E.W.; Jacobsen, R.T. Viscosity and thermal conductivity equations for nitrogen, oxygen, argon, and air. *Int. J. Thermophys.* **2004**, *25*, 21–69. [[CrossRef](#)]
43. Sosnowski, M.; Krzywanski, J.; Grabowska, K.; Gnatowska, R. Polyhedral meshing in numerical analysis of conjugate heat transfer. In *EPJ Web of Conferences*; EDP Sciences: Ulis, France, 2018; Volume 180, p. 02096.
44. Symscape. Polyhedral, Tetrahedral, and Hexahedral Mesh Comparison. Available online: <https://www.symscape.com/polyhedral-tetrahedral-hexahedral-mesh-comparison> (accessed on 17 June 2020).

45. Abdallah, A.; Krameldin, A. Optimum thermal design of steam pipelines and its impact on environment pollution. In Proceedings of the Conference on Heat Exchangers Boilers and Pressure Vessels, Cairo, Egypt, 3–5 October 1999; pp. 57–74.
46. Ghalambaz, M.; Abdollahi, M.; Eslami, A.; Bahrami, A. A case study on failure of AISI 347H stabilized stainless steel pipe in a petrochemical plant. *Case Stud. Eng. Fail. Anal.* **2017**, *9*, 52–62. [[CrossRef](#)]



© 2020 by the authors. Licensee MDPI, Basel, Switzerland. This article is an open access article distributed under the terms and conditions of the Creative Commons Attribution (CC BY) license (<http://creativecommons.org/licenses/by/4.0/>).